Martin *et al*, 2002). For those techniques, waking animal experiments that require the animal to be trained to tolerate restraint in a holder and experimental set-up have been established (Berwick *et al*, 2002; Martin *et al*, 2002). Compared with other imaging methods, one major advantage that optical imaging techniques offer in neurovascular coupling studies is that they allow for imaging of neural activity on a mesoscopic scale similar to that of the hemodynamic imaging accomplished by measuring activity-induced changes in membrane potentials (Obrenovitch *et al*, 2009; Takashima *et al*, 2001; Ebner and Chen, 1995), intracellular pH (Sun *et al*, 2011), calcium ion concentrations (Homma *et al*, 2009) combined with exogenous fluorescent compounds, and endogenous fluorescent changes arising from activity-dependent cellular autofluorescence (Reinert *et al*, 2007; Shibuki *et al*, 2003). These techniques enable us to directly examine the spatial gaps between neural and vascular response regions (Weber *et al*, 2004). More directly, the *in-vivo* microscopic morphology and function of neurons, astrocytes, pericytes, and capillaries are resolved at the single-cell level with laser scanning fluorescent microscopic techniques, including confocal (Seylaz *et al*, 1999; Villringer *et al*, 1994) and two-photon excitation fluorescence microscopy (Fernández-Klett *et al*, 2010; Göbel and Helmchen, 2007; Takano *et al*, 2006; Chaigneau *et al*, 2003; Kleinfeld *et al*, 1998). In these techniques, image quality is sensitive to animal vibration, and thus, imaging is preferably conducted under anesthesia. A recent study showed that, in two-photon microscopic experiments, the image distortion was minimized to 2 to 5 μm in waking conditions by fixing animal's head to the stage and allowing the animal to move freely on a floating ball (Dombeck *et al*, 2007). This report indicates the feasible image resolution for examining neurovascular coupling in awake animals. Miniaturized two-photon microscopy has also been shown to capture images of cortical cells and capillary blood flow under unanesthetized conditions (Helmchen, 2002), which could be useful in future studies of cellular-scale neurovascular coupling in freely behaving animals.

Why Do We Need to Care About Anesthesia?

Different anesthetics have different action sites, which can potentially cause discrepancies in interpreting the mechanism of neurovascular coupling due to animal experiments conducted with different anesthetics. It was shown that intravenous infusion of cocaine in anesthetized rats provoked an increase in CBF under α-chloralose (25 mg/kg per hour), but the same experiments conducted under isoflurane (1.8% to 2.0%) showed decreases in CBF (Du *et al*, 2009). The cerebrovascular response to ethanol was shown to cause vasoconstriction under α-chloralose/urethane anesthesia (50/600 mg/kg) but vasodilation under halothane (0.5% to 1.0%) (Gordon *et al*, 1995). Furthermore, the role of the nitric oxide pathway in controlling CBF response to sensory stimulation was shown to be dominant in anesthetized rats (urethane, Gerrits *et al*, 2001; α-chloralose 40 mg/kg per hour, Nakao *et al*, 2001). However, when examined in awake rats, this nitric oxide pathway does not have a major role (Nakao *et al*, 2001). These findings indicate that particular anesthetics critically interfere with the pathway of neurovascular coupling.

Another issue concerning the use of anesthesia in neurovascular coupling experiments is that anesthesia profoundly affects the stability and reproducibility of neurovascular imaging. Austin *et al* (2005) showed that fMRI blood oxygen level-dependent responses to sensory stimulation varied over 6 hours of measurements in rats under α-chloralose (10 to 30 mg/kg per hour), accompanied with the varying electroencephalogram. However, in rats under urethane anesthesia (1.1 g/kg), electroencephalogram activity was shown to be stable for a prolonged time (8 to 12 hours) (Lincoln, 1969). To maintain steady electroencephalogram and fMRI responses with rats receiving medetomidine infusion (0.1 to 0.3 mg/kg per hour), the infusion rate needs to be adjusted over time due to potential pharmacokinetic changes in long-term experiments (>3 hours) (Pawela *et al*, 2009). Moreover, functional connectivity examined with blood oxygen level-dependent fMRI was well localized in rats anesthetized with either α-chloralose (27 mg/kg per hour) or medetomidine (0.1 mg/kg per hour) but less so under isoflurane (2%) (Williams *et al*, 2010). These reports indicate that choosing the appropriate anesthesia and adjusting its dosage are critical for achieving stable and reproducible experimental conditions. In the following sections, we will discuss the effects of anesthesia on the major properties of neurovascular coupling: (1) the spatial coordination of the vascular response with respect to the neurally derived map; (2) the temporal dynamics; and (3) the quantitative relationships examined under a variety of anesthesia conditions compared with those under unanesthetized conditions.

Anesthesia interference with neurovascular coupling

Spatial Coordination

Anesthesia-dependent variations in cortical mapping with OIS (630 nm) based on fingerpad stimulation were reported in the monkey somatosensory cortex (pentothal 1 to 2 mg/kg per hour versus isoflurane 0.8% to 1.5%) (Chen *et al*, 2001). In this study, mapping under pentothal produced focal localization, whereas maps obtained under isoflurane were less uniform and more broad. This observation was thought to occur because pentothal has suppressive actions on cortical activity due to both the

potentiation of GABAergic interneurons and the suppression of the excitability of glutamatergic neurons, whereas isoflurane enhances surround inhibition (Chen *et al*, 2001). Although the effects of focal excitation and surround inhibition on hemodynamic regulation are not fully understood (Boorman *et al*, 2010; Devor *et al*, 2007), the observed variation of the cortical mapping could depend on the actions of the anesthesia on both the neural and vascular components. Enhanced stimulus-specific localization of the cerebral blood volume (CBV)-weighted OIS (570 nm) under waking conditions relative to anesthetized conditions was observed for orientation column mapping in the cat visual cortex (Fukuda *et al*, 2005). Shtoyerman *et al* (2000) suggested that the increased specificity for the CBV response is due to an increased vascular response and signal transmission from neurons to vessels at the active columns because of the relatively unchanged spatial properties of neural responses. With increased focal activity, one may expect that the CBF/CBV response region would expand due to the activity-dependent spread of the vasodilation region (Kannurpatti and Biswal, 2011; Masamoto *et al*, 2010*a*; Durduran *et al*, 2004). However, enhanced surround inhibition may also cause vasoconstriction in that region (Devor *et al*, 2007), leading to a sharp tuning of the CBF/CBV supply to the focal active region.

To further explore the spatial gap between vascular response regions and activated neural sites at the cellular scale of the spatial resolution, Chaigneau *et al* (2003, 2007) applied two-photon imaging techniques to a rodent olfactory bulb model. A series of experiments showed that no tight coupling exists between activated glomeruli, and nearby capillary flow changes depending on inducing odor stimuli in rats or mice (either urethane 1.5 g/kg or ketamine/xylazine 90/10 to 100/16 mg/kg, Jukovskaya *et al*, 2011; Chaigneau *et al*, 2007). Based on these findings, it was suggested that the spatial mismatch originates from a vascular mechanism, such as the nonspecific orientation of capillaries, which pass through several neural modules. Furthermore, this spatial mismatch may also be related to the regulatory mechanism of capillary blood flow in which control may not be localized within a single capillary. The findings further suggest a role for precapillary arterioles in controlling capillary blood flow during cortical activation (Fernández-Klett *et al*, 2010). Overall, anesthesia interference with spatial CBF coordination could be caused by both anesthesia-dependent modulation of neural processing, such as local balance between excitatory and inhibitory activity, and changes in vascular response sensitivity to underlying neural activity. However, the mechanisms that (1) detect focal excitatory and surrounding inhibitory activity in neighboring capillaries, (2) transport the vasoactive signals to upstream parent arteries (arterioles), and (3) control CBF balances between the active and inactive regions remain unknown.

Temporal Dynamics

The factors affecting the time delay in the vascular response relative to the onset of a neural response are the following: (1) the release of vasoactive signals from neurons, (2) the transmission of the signals, (3) the uptake of the signals by vascular cells, and (4) the action of the vascular cells. Hayton *et al* (1999) reported that the onset latency of somatosensory-evoked potential after electrical stimulation to rat paws was slightly changed by anesthesia: 8.2 ± 5.0 ms for ketamine/xylazine (90/10 mg/kg), 7.5 ± 3.5 ms for medetomidine (0.3 mg/kg), 5.4 ± 2.6 ms for isoflurane (2%), and 6.3 ± 2.6 ms for fentanyl/fluanisone-midazolam (0.85/27 and 13.5 mg/kg, respectively), after the onset of forelimb stimulation. Dose-dependent increases in the latency of somatosensory-evoked potential (1.8 ± 0.8 ms per % isoflurane concentration) have also been observed in human subjects with inhaled anesthetics (0% to 1.65% isoflurane) (Sebel *et al*, 1986). These reports showed that the effect of anesthesia on the temporal dynamics of synaptic transmission is relatively small, indicating minimum interference with the latency of vasoactive signal release (i.e., within a couple of milliseconds).

An early study using an impedance technique suggested that the earliest onset of evoked vasodilation in response to auditory stimulation is ~0.15 to 0.25 seconds from the onset of neural activation in conscious human brains (Sandman *et al*, 1984). In accordance with this observation, Nielsen and Lauritzen (2001) reported that the earliest onset latency of laser-Doppler flowmetry response measured in upper cortical layers was 0.2 ± 0.2 seconds after infraorbital nerve stimulation in anesthetized rats (α-chloralose 45 to 60 mg/kg per hour). Short onset latencies (0.2 to 0.4 seconds) of the red blood cell speed change after sensory stimulation were also observed in the parenchymal capillaries of awake mice with two-photon microscopy (Drew *et al*, 2011). These observations are also in good agreement with the reported onset time of the earliest plasma volume increases (< 0.5 second latency) that originate from the arterioles of the middle cortical layers (α-chloralose 40 mg/kg per hour) (Tian *et al*, 2010), and the CBV onset (0.35 second) that starts from middle cortical layers measured with fMRI in rats (α-chloralose 26.7 mg/kg per hour) (Hirano *et al*, 2011). Considering these small variations in the reported onset latency of evoked vasodilation and capillary red blood cell speed changes, it can be expected that the transmission of vasodilatory signals to vascular cells is minimally influenced by anesthesia (e.g., α-chloralose) or has minimal variations that are not detectable with current methodologies. Because the frame rates of the MRI and two-photon imaging conducted in those studies were reported to be 4 and 5 to 30 frames per second, respectively, these resolutions may be not sufficient to stably track the fast responses of the vascular reaction. Furthermore,

Table 1 Onset delay of hemodynamic response relative to neural response in rats

Onset time (seconds)	*Criteria*	*Anesthetic (dosage)*	*Stimulation (pulse width, current, frequency)*	*Measurement*	*Reference*
1.8 ± 0.2	> 2 s.d.	Ure (1.5 g/kg)	Odor (2 seconds)	Two-photon MS (capillary RBC speed)	Chaigneau *et al* (2003)
0.50 ± 0.10 0.63 ± 0.25 0.56 ± 0.19	Intersection of initial slope	Ure (1.25 g/kg)	WP (0.3 ms, 1.2 mA, 5 Hz)	OIS (parenchyma) OIS (artery) OIS (vein)	Berwick *et al* (2005)
0.7 ± 0.1	Not clear	Ketamine (6 mg/kg)	Whisker (2 Hz, 10 seconds)	H_2 clearance	Khananashvili and Demidova (2002)
0.2 ± 0.2	> 2 s.d.	AC (45–60 mg/kg per hour)	Infraorbital nerve (1 ms, 1.5 mA, 2 Hz)	LDF	Nielsen and Lauritzen (2001)
0.34 ± 0.06	Intersection of initial slope	AC (35 mg/kg per hour)	Cortex (1 ms, 10–15 μA, 5–50 Hz)	LDF	Matsuura *et al* (1999)
0.4 ± 0.1	> 2 s.d.	AC (30 mg/kg per hour)	HP (1 ms, 1.2 mA, 2–20 Hz)	LDF	Sheth *et al* (2005)
0.52 ± 0.06	Intersection of initial slope	AC (45 mg/kg per hour)	HP (0.1 ms, 1.5 mA, 5 Hz)	LDF	Matsuura *et al* (2000)
0.54 ± 0.07 0.75 ± 0.13	Statistical analysis	AC (40 mg/kg per hour)	FP or HP (3 ms, 1 mA, 3 Hz)	OIS (parenchyma) OIS (artery)	Chen *et al* (2011)
< 0.5	Intersection of initial slope	AC (40 mg/kg per hour)	FP (0.3 ms, 1 mA, 3 Hz)	Two-photon MS (plasma volume)	Tian *et al* (2010)
0.7 ± 0.4	> 1 s.d.	AC (27 mg/kg per hour)	FP (0.3 ms, 1.5 mA, 3 Hz)	fMRI (CBF)	Silva *et al* (2000)
0.40 ± 0.22 0.43 ± 0.18 0.61 ± 0.34	> 1 s.d.	AC (27 mg/kg per hour)	Bilateral forelimb (0.3 ms, 2 mA, 3 Hz)	fMRI (CBF, layers I–II) fMRI (CBF, layers III–V) fMRI (CBF, layer VI)	Hirano *et al* (2011)
0.34 ± 0.19 0.35 ± 0.16 0.58 ± 0.25	> 1 s.d.	AC (27 mg/kg per hour)	Bilateral forelimb (0.3 ms, 2 mA, 3 Hz)	fMRI (CBV, layers I–II) fMRI (CBV, layers III–V) fMRI (CBV, layer VI)	Hirano *et al* (2011)
1.3	30% peak	AC (30–40 mg/kg per hour)	FP (3 ms, 1.6 mA, 3 Hz)	OIS (total Hb)	Hillman *et al* (2007)
0.4–0.6	Intersection of initial slope	Iso (1.4%)	FP (1.0 ms, 1.0 mA, 2–20 Hz)	LDF	Masamoto *et al* (2007)

AC, α-chloralose; CBF, cerebral blood flow; CBV, cerebral blood volume; fMRI, functional magnetic resonance imaging; FP, forepaw; HP, hindpaw; Iso, isoflurane; LDF, laser-Doppler flowmetry; MS, microscope; OIS, optical intrinsic signal; RBC, red blood cell; s.d., standard deviation; Ure, urethane; WP, whisker pad.

additional tests of other cortical regions and with different anesthetics are also needed.

Moreover, the definition of the onset timing of the evoked vascular response may be biased depending on the criteria by which threshold levels for activity-induced changes are determined relative to baseline fluctuations (e.g., a threshold at twofold the standard deviation of baseline or an intersection between baseline and initial slope). Nevertheless, we found that the literature showed narrow ranges for the onset time (0.2 to 0.7 seconds) of evoked CBF in the rat somatosensory cortex regardless of the criteria used to define onset time under α-chloralose (Hirano *et al*, 2011; Sheth *et al*, 2005; Nielsen and Lauritzen, 2001; Silva *et al*, 2000; Matsuura *et al*, 1999, 2000). These findings are also in good agreement with the results measured under isoflurane anesthesia (0.4 to 0.6 seconds; Masamoto *et al*, 2007; Table 1). In contrast, relatively variable reports were found for the onset time of CBV changes (0.5 to 1.3 seconds) with OIS in a rat somatosensory model (α-chloralose, Chen *et al*, 2011; Hillman *et al*, 2007, versus urethane, Berwick *et al*, 2005). The large variations observed in the OIS results could be related to technical issues concerning spectral decomposition to calculate total hemoglobin content and the different signal-to-noise ratios of the measurements. Differing regions of interest also potentially contributed to the observed discrepancies, as it is well known that CBV changes spread along the vasculature from the activated hot spots (Chen *et al*, 2011; Sheth *et al*, 2005).

Whether certain anesthetics directly interfere with the dynamics of vascular responses (e.g., the propagation speeds of the vasodilatory signals) remains incompletely understood. In rats anesthetized with urethane (1.25 g/kg), the times-to-peak of CBF responses were observed to be longer (0.6 to 1.2 seconds) than those observed under waking conditions (Martin *et al*, 2006). In contrast, a similar time course of evoked change was observed for arterial vascular responses measured under either awake or urethane anesthesia (1 g/kg) conditions in the mouse somatosensory cortex (Drew *et al*, 2011). Although the cause of the controversial results (i.e., urethane effects) remains unclear in those studies, anesthesia may affect the temporal dynamics of vascular responses in varying degrees via its actions on the intracellular

calcium dynamics of smooth muscle cells and the reactivity to the vasoactive substances (Altura *et al*, 1980), and secondary effects via anesthesia-induced changes in systemic conditions, such as hypercapnia and hypotension.

Quantitative Relationships

The quantitative coupling relationships between evoked neural and vascular responses are largely influenced by the anesthesia. The route of this action involves anesthesia-dependent modulation of the following: (1) neural processing, (2) the vasoactive signal pathway, and (3) vascular cell reactivity. In awake conditions, larger evoked CBF/CBV changes have generally been observed than those observed in anesthetized conditions (Fukuda *et al*, 2005; Martin *et al*, 2006). Simultaneous recordings of evoked neural and vascular responses in rats have shown that the reduced hemodynamic responses under anesthesia (urethane 1.25 g/kg) were mainly due to the suppression of cortical excitability (Martin *et al*, 2006). The suppression of cortical activity is thought to be due to the suppression of thalamocortical inputs and suppression of cortical processing. Franceschini *et al* (2010) showed strong reduction of thalamocortical input under either ketamine/xylazine (20/2 mg/kg per hour) or fentanyl/droperidol (0.09/4.5 mg/kg per hour) anesthesia measured with somatosensory-evoked potential (i.e., a first positive peak, P1) in rats, whereas relatively preserved thalamocortical input was observed with α-chloralose (40 mg/kg per hour). Either pentobarbital (25 mg/kg) or propofol (50 mg/kg per hour) preserved thalamocortical inputs but reduced cortical activity, leading to the lowest hemodynamic responses among the anesthesia conditions tested (Franceschini *et al*, 2010). These findings strongly indicate that the reduced magnitude of cortical vascular response under general anesthesia originates from the anesthesia-dependent modulation of cortical processing.

In the rat primary somatosensory cortex, it was shown that anesthesia profoundly affects neural refractory periods with different degrees of potentiation depending on the anesthesia type and dosage (Masamoto *et al*, 2007, 2009). A prolonged refractory period was observed under α-chloralose (Masamoto *et al*, 2007; Ogawa *et al*, 2000), whereas short refractory periods were maintained under isoflurane and enflurane anesthesia. The latter anesthetics maintained robust hemodynamic responses to higher frequency stimulation (6 to 10 Hz; Kim *et al*, 2010; Masamoto *et al*, 2007; Sheth *et al*, 2003), which is in contrast to the well-known frequency dependencies in the rat somatosensory models using α-chloralose (a peak at a frequency of 1.5 to 5 Hz; Table 2). In addition, under different levels of isoflurane (0.8% to 2.2%), cortical adaptation was enhanced in a dose-dependent manner (Masamoto *et al*, 2009). In this condition, the evoked CBF induced by single-pulse local field potential (i.e., hemodynamic impulse response) was, however, found to increase in a dose-dependent manner (Masamoto *et al*, 2009). As a result, the optimum stimulus frequency that evoked the highest CBF response per given stimulus duration was shifted from high to low frequency stimulation with increases in anesthesia depths (Masamoto *et al*, 2009). Strong cortical adaptation under isoflurane (1.2%) was also consistently found in the rat somatosensory model with diffuse optical imaging (Franceschini *et al*, 2010). In this study, the highest hemodynamic response per given neural activity (P2 or N1 of somatosensory-evoked potential) was observed for either α-chloralose (40 mg/kg per hour) or isoflurane (1.2%), while a 10-fold higher CBF response to CO_2 challenges (5% CO_2 gas) was observed for isoflurane compared with ketamine/xylazine, propofol, or α-chloralose anesthesia (Franceschini *et al*, 2010). These findings suggest that separate mechanisms are involved in the vasodilatory response to neural stimulation and CO_2 challenge. In conclusion, the effects of anesthesia on quantitative neurovascular coupling primarily consist of the modulation of cortical processing and, thus, vasoactive pathways, while the effects of vascular reactivity differences on evoked vascular responses are weaker and the degree of these effects depends on anesthesia type and depth. Because different stimulus frequencies (4 to 30 Hz) were shown to evoke different populations of excitatory pyramidal cells and vasoactive inhibitory interneurons (Enager *et al*, 2009), it is likely that this anesthesia interference with cortical processing involves actions on the variable populations of vasoactive local interneurons (Lecrux *et al*, 2011; Harris *et al*, 2010). The cellular mechanism of the anesthesia action and its involvement in neurovascular transmission must be better identified in future studies.

Sites of action of anesthesia and neurovascular coupling

The potential target sites of anesthesia actions involved in neurovascular coupling are summarized in this section with emphasis on the anesthetics frequently used in animal experiments of neurovascular coupling and imaging, such as α-chloralose, isoflurane, pentobarbital, urethane, and medetomidine. The appropriate dosages and type of anesthetic for acute and chronic experiments in both rats and mice can be referenced in the literature (Lukasik and Gillies, 2003).

General Physiology

Alpha-chloralose is thus far the most commonly used anesthesia in neurovascular coupling imaging and physiology experiments in rodents because the early studies have shown that this agent preserves

Table 2 Stimulation frequency dependences of hemodynamic responses in rat somatosensory cortex

Optimum frequency (Hz)	*Anesthetic (dosage)*	*Stimulation (pulse width, current)*	*Range of frequency (Hz)*	*Stimulation duration (seconds)*	*Techniques*	*Reference*
40	Waking	WP (0.3 ms, 0.3 mA)	1–40	2	LDF	Martin *et al* (2006)
5	Ure (1.25 g/kg)	WP (0.3 ms, 1.2 mA)				
3	Ure (1 g/kg)	WD (1 mm)	1–20	60	H_2 clearance	Moskalenko *et al* (1996)
5	Etomidate (1.5–2.1 mg/kg per hour)	WD (maximum)	1–7	120	ARG (^{14}C-IAP)	Vogel and Kuschinsky (1996)
10.5	Ure (1.2 g/kg)	WD (5 mm)	1.5–10.5	15	LDF	Gerrits *et al* (1998)
10	Ure (1.2 g/kg)	WAP (15 ms)	1–10	44	2D-LDFI	Kannurpatti and Biswal (2011)
12	AC (40 mg/kg per hour)	WAP (16.7–125 ms)	4–30	30	fMRI (BOLD)	Sanganahalli *et al* (2008)
1.5		FP (0.3 ms, 2 mA)	0.5–30			
9–15	Ure (1.25 g/kg)	FP (0.3 ms, 1–1.2 mA)	1–15	30	fMRI (BOLD)	Huttunen *et al* (2008)
10	Enf (1–2%)	HP (1.0 ms, 1.0 mA)	2–20	2	OIS (570 nm)	Sheth *et al* (2003)
12	Iso (1.4%)	FP (1.0 ms, 1.0 mA)	2–20	0.5–5	LDF and fMRI	Masamoto *et al* (2007)
6–8	Iso (1.3–1.5%)	FP (1.0 ms, 1.5 mA)	1–24	30	LDF and fMRI	Kim *et al* (2010)
9	Med (0.1 mg/kg per hour)	FP (0.3 ms, 2 mA)	1–18	20	fMRI (BOLD)	Zhao *et al* (2008)
8	K/X (75/5 mg/kg)+ AC (60 mg/kg)	BiFP (10 ms, 1 mA)	1–12	40	fMRI (BOLD)	van Camp *et al* (2006)
3	AC (27 mg/kg per hour)	BiFP (0.3 ms, 2 mA)	1–8	45	fMRI (BOLD)	Keilholz *et al* (2004)
2	AC (30 mg/kg per hour)	HP (1.0 ms, 0.8 mA)	2–20	2	LDF and OIS	Sheth *et al* (2004)
5	AC (45 mg/kg per hour)	HP (0.1 ms, 1.5 mA)	0.2–10	5	LDF	Matsuura and Kanno (2001)
3	AC (27 mg/kg per hour)	FP (0.3 ms, 1.5 mA)	1–5	40	LDF	Silva *et al* (1999)
1.5	AC (27 mg/kg per hour)	FP (0.3 ms, 0.5 mA)	1.5–6	50	fMRI (BOLD)	Brinker *et al* (1999)
1.5	AC (27 mg/kg per hour)	FP (0.3 ms, 0.5 mA)	1.5–9	40	fMRI (BOLD)	Gyngell *et al* (1996)

AC, α-chloralose; ARG, autoradiography; BiFP, bilateral forepaw; BOLD, blood oxygen level-dependent; ^{14}C-IAP, [^{14}C]iodoantipyrine; 2D-LDFI, two-dimensional laser-Doppler flowmetry imaging; Enf, enflurane; fMRI, functional magnetic resonance imaging; FP, forepaw; HP, hindpaw; Iso, isoflurane; K/X, ketamine/xylazine; LDF, laser-Doppler flowmetry; Med, medotomidine; OIS, optical intrinsic signal; Ure, urethane; WAP; whisker air-puff; WD, whisker deflection; WP, whisker pad.

robust and stable hemodynamic and metabolic coupling to sensory stimulation (Lindauer *et al*, 1993; Ueki *et al*, 1992). The effects of α-chloralose on general physiology include respiratory depression, metabolic acidosis, and hyperreactivity (Arfors *et al*, 1971). The analgesic properties of this agent are questionable (Silverman and Muir, 1993), and thus, any surgical preparation must be performed with administration of another anesthetic. This procedural complication before the experiment contributes to the variable results regarding neurovascular coupling relationships in α-chloralose-anesthetized rats (Bonvento *et al*, 1994). In addition, the use of α-chloralose is limited to experiments with nonsurvival protocols (Silverman and Muir, 1993), which hampers the use of this animal model for wider applications, such as repeated longitudinal experiments.

Alternatively, several groups have introduced inhaled anesthetics (e.g., halothane, enflurane, and isoflurane) for rodent neurovascular coupling studies (Kim *et al*, 2010; Masamoto *et al*, 2007; Schulte and Hudetz, 2006; Sheth *et al*, 2003). A major advantage of inhaled anesthetics is that the fast induction and rapid recovery achieved with these anesthetics make them usable for repeated longitudinal experiments. However, a known disadvantage of these agents is that volatile anesthetics themselves are potent vasodilators and, thus, cause cerebral vasodilation, which leads to increased baseline CBF that is uncoupled from the cerebral energy metabolism (van Aken and van Hemelrijck, 1991). The effects might be more severe in mice compared with rats. Moreover, it was shown that high concentrations of isoflurane (>3%) break down the cortical blood–brain barrier (Tétrault *et al*, 2008), and isoflurane impairs glucose-stimulated insulin release (Tanaka *et al*, 2011).

Barbiturate anesthetics, including pentobarbital and thiopental, suppresses cardiac output and often cause hypotension. Respiratory depressant effects of pentobarbital have also been reported (Field *et al*, 1993). In contrast, urethane provides moderate depression of blood pressure and heart rate, and may cause hyperventilation (Field *et al*, 1993). Intraperitoneal administration of urethane (1.2 g/kg) was shown to cause hyperglycemia associated with hypothalamic activation (Reinert, 1964; Maggi and Meli, 1986). Urethane is also known as potential mutagen and carcinogen (Field and Lang, 1988). Medetomidine and xylazine are specific α2-adrenoreceptor agonists that block norepinephrine release. Due to the limited analgesic properties of these agents, surgical procedures should be performed in combination with other anesthetic agents. The α2-adrenoreceptor was also known to significantly affect cardiovascular function and depress respiratory

function (Sinclair, 2003). Animals can recover after the administration of a reversible α2-antagonist, making this agent also suitable for use in repeated longitudinal imaging experiments (Pawela *et al*, 2009; Weber *et al*, 2006).

Neural Activity

The action sites at which anesthesia influences neural pathways have been shown to involve common targets, such as ligand-gated ion channels (potentiation of GABA type A and glycine receptors, and suppression of NMDA (*N*-methyl-D-aspartate) receptor) and presynaptic actions on calcium, potassium, and sodium channels (for reviews, see Chau, 2010; Hemmings 2009; Franks, 2008). Isoflurane was shown to predominantly reduce presynaptic excitability via sodium channel blockade (Hemmings 2009) and, thus, glutamate release (Sandstrom, 2004; Wu *et al*, 2004). Moreover, the inhibition of the NMDA receptor, potentiation of GABA type A receptors, and suppression of acetylcholine transmission and receptors have also been reported (Dickinson *et al*, 2007; Hentschke *et al*, 2005; Violet *et al*, 1997).

The action site of α-chloralose has been shown to involve the potentiation of GABA-induced currents by increasing affinity for GABA (Garrett and Gan, 1998), whereas preserved synaptic transmission and glutamate-, glycine-, and acetylcholoine-induced current were observed at low concentration of α-chloralose (Wang *et al*, 2008). Pentobarbital binds to GABA type A receptors and enhances GABA-mediated inhibitory neurotransmission (Curtis and Lodge, 1977). Pentobarbital and thiopental have also been shown to inhibit the release of acetylcholine, norepinephrine, and glutamate (Nicoll, 1978; Curtis and Lodge, 1977). Significant inhibition of the alpha-amino-3-hydroxy-5-methyl-4-isoxazolepropionic acid receptor by pentobarbital has also been found, but pentobarbital has small effects on NMDA, glycine, and GABA receptors (Hara and Harris, 2002). Medetomidine selectively inhibits noradrenergic neurons in the locus coeruleus and has been shown to disrupt thalamocortical transmission (Sinclair, 2003). Urethane is shown to have modest effects on multiple ligand-gated ion channels, including potentiation of GABA type A and glycine receptors, and mild inhibition of NMDA and alpha-amino-3-hydroxy-5-methyl-4-isoxazolepropionic acid receptors (Hara and Harris, 2002; Maggi and Meli, 1986; Minchin, 1981), which shows that this agent is suitable for pharmacological studies of neurotransmitter release and uptake.

Vasoactive Signal Transmission

Determining the action site on neural processing and the resultant effects on the vascular responses would provide an insight into the mechanism of the neurovascular transmission pathway. However, it is difficult to directly identify and purify the action site of anesthesia because most neurovascular transmissions share a common mechanism of neural processing. Volatile anesthetics, but not ketamine or pentobarbital, have been shown to enhance glutamate uptake by astrocytes (Miyazaki *et al*, 1997), and dose-dependent closure of astrocytic gap junctions has been observed with volatile anesthetics in cultured astrocytes (Mantz *et al*, 1993). Whether these effects of isoflurane on astrocyte function are related to the observed dose-dependent increase in hemodynamic impulse responses (Masamoto *et al*, 2009) remains unclear. Future studies should determine the exact contribution of the actions of anesthetics on astrocyte mechanisms using pharmacological approaches. Furthermore, experimental models with well-defined neural circuits would be useful to further determine the action site in *in-vivo* conditions and its contribution to the generation of the blood oxygen level-dependent fMRI signal (Krautwald and Angenstein, 2012).

Vascular Responses

Some anesthetics have been shown to directly affect vascular physiology. Isoflurane dose dependently induced the relaxation of cerebral arteries (i.e., vasodilation) via its actions on ATP-sensitive potassium channels and reduced calcium current in smooth muscle cells (Iida *et al*, 1998; Flynn *et al*, 1991, 1992). In contrast, endothelium-dependent vasodilation induced by acetylcholine was inhibited by isoflurane due to its inhibiting effects on formation of nitric oxide in endothelium (Nakamura *et al*, 1994; Toda *et al*, 1992). Autoregulatory responses, and the CBF response to CO_2 inhalation, were shown to be preserved under isoflurane anesthesia (Lee *et al*, 1994, 1995). However, a depression of the vascular response to CO_2 inhalation has been found in rats anesthetized with 2% isoflurane compared with the waking condition (Sicard *et al*, 2003). It is well known that pentobarbital causes a reduction of CBF relative to awake conditions (Wei *et al*, 1993). However, the effects of barbiturate anesthetics on cerebral vessels have been shown to be controversial; they can act as potent vasoconstrictors (Tsuji and Chiba, 1987) or vasodilators (Ogura *et al*, 1991). Medetomidine also causes α2-adenoreceptor-mediated vasoconstriction of cerebral arteries and results in reduced CBF (Sinclair, 2003; Ganjoo *et al*, 1998). Decreased sensitivity of the cerebrovascular response to arterial CO_2 has been reported for α-chloralose (100 mg/kg; Sándor *et al*, 1977). Furthermore, we observed that the capillary diameter in the resting state was slightly larger under 45 mg/kg per hour α-chloralose ($5.1 \pm 1.2\,\mu$m) than 1.4% isoflurane ($4.8 \pm 1.1\,\mu$m) (Masamoto *et al*, 2010*b*), which may further contribute to the anesthesia-dependent variations of microvascular responses to physiological perturbations, such as the contribution of capillary diameter changes measured under different anesthesia conditions.

Other Considerations

As discussed above, one should consider the effect of anesthesia on baseline (prestimulus resting) conditions. It has been reported that activation-induced changes of brain activity were largely dependent on the baseline states, such as the anesthesia-dependent reduction of oxygen and glucose metabolism and unit neural activity (Hyder *et al*, 2002; Shulman *et al*, 1999). In these studies, lower baseline states induced by anesthesia have been shown to cause larger activation changes. Because the resting-state energy metabolism is known to be coupled to baseline CBF, it can therefore be expected that baseline CBF also differs depending on the anesthesia. Some previous works regarding the baseline CBF measured under a variety of anesthesia conditions in the rat cerebral cortex are summarized in Table 3. Overall, injectable anesthetics (α-chloralose and pentobarbital) reduced baseline CBF, whereas low concentration of isoflurane (1.3% to 1.5%) maintained CBF values close to those of the awake condition (Table 3). Whether these modulatory effects of anesthesia on baseline CBF affect activation-induced vascular responses remains relatively unknown (Franceschini *et al*, 2010). However, caution should be exercised in comparing the quantitative data examined under different baseline states with different anesthesia.

Finally, repeated longitudinal experiments are becoming increasingly more important for further understanding the biological implications and plasticity of neurovascular coupling (Brown *et al*, 2010; Colonnese *et al*, 2008). For longitudinal experiments, the same anesthetics have been repeatedly used in single animals; i.e., isoflurane (Colonnese *et al*, 2008; Tomita *et al*, 2005) and ketamine/xylazine (Brown *et al*, 2010). For those experiments, good recovery from anesthesia discontinuation is important in the choice of anesthetics for performing controlled experiments. Hayton *et al* (1999) reported that ketamine/xylazine, medetomidine, and fentanyl/fluanisone-midazolam cause losses in body weight; however, isoflurane does not have this effect. No effects on cell proliferation were found for isoflurane, propofol, medetomidine, or ketamine in young rats (Tung *et al*, 2008); these results are particularly important for developmental and regeneration studies with long-term imaging experiments.

Summary

The effects of anesthesia on neurovascular coupling involve the following: (1) changes in general physiology, (2) direct interference with cortical neural processing, (3) modulation of vasoactive signal transmission, and (4) suppression of vascular cell activities (Figure 2). It is well known that anesthesia modifies the balance between focal excitation and surround inhibition in a manner dependent on the type and dosage of anesthesia. However, the resultant effects on spatial coordination of vascular responses, such as activity-dependent vasodilation and vasoconstriction, are not well understood. Propagation time, in particular that for the onset latency of vasodilation evoked by neural stimulation, is relatively preserved across anesthesia states (Table 1), but

Table 3 Baseline CBF in rat cortex

CBF (ml/100 g per minute)	*Anesthetic (dosage)*	*Region*	*Technique*	*Reference*
167 ± 45	Waking	Sensorimotor	ARG (^{14}C-IAP)	Kuschinsky *et al* (1985)
155 ± 30	Waking	Sensorimotor	ARG (^{14}C-IAP)	Maekawa *et al* (1986)
102 ± 35	Iso (0.7%)			
147 ± 40	Iso (1.4%)			
183 ± 63	Iso (2.1%)			
247 ± 67	Iso (2.8%)			
134 ± 8	Waking	Sensorimotor	ARG (^{14}C-IAP)	Lenz *et al* (1998)
132 ± 26	Iso (1.4%)			
153 ± 14	Iso (2.8%)			
151 ± 23	Iso (1.3–1.5%)	Somatosensory	MRI (ASL)	Kim *et al* (2007)
146 ± 13	Ure (1.2 g/kg)	Somatosensory	ARG (^{14}C-IAP)	Gerrits *et al* (2000)
168 ± 12	Waking	Sensorimotor	ARG (^{14}C-IAP)	Otsuka *et al* (1991)
55 ± 5	Pen (50 mg/kg)			
180 ± 15	Waking	Somatosensory	ARG (^{14}C-IAP)	Nakao *et al* (2001)
65 ± 5	AC (40 mg/kg per hour)			
58 ± 3	AC (26.7 mg/kg per hour)/50%N_2O	Cortex	MRI (CASL)	Lee *et al* (2001)
75 ± 9	Morphine (60 mg/kg per hour)/70% N_2O	Somatosensory	MRI	Hyder *et al* (2000)
40 ± 9	AC (40 mg/kg per hour)/70% N_2O			
90 ± 20	AC (36 mg/kg per hour)/70% N_2O	Somatosensory	MRI	Smith *et al* (2002)
60 ± 20	AC (46 mg/kg per hour)/70% N_2O			

AC, α-chloralose; ARG, autoradiography; ASL, arterial spin labeling; CASL, continuous arterial spin labeling; CBF, cerebral blood flow; ^{14}C-IAP, [^{14}C]iodoantipyrine; Iso, isoflurane; MRI, magnetic resonance imaging; Pen, pentobarbital.

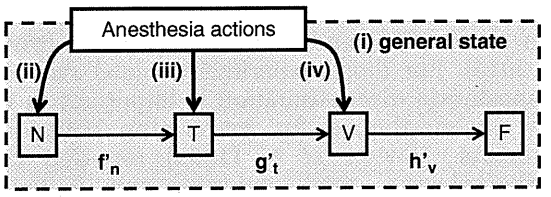

(i) Systemic physiology
- blood gas conditions
- cardiac output
- arterial blood pressure

(iii) Vasoactive signal Transmission
- release and uptake of transmitters
- efficiency of transmission
- turnover

(ii) Neural activity
- synaptic transmission
- pre-synaptic release
- post-synaptic receptors
- removal of transmitters
- membrane potentials

(iv) Vascular reactivity
- baseline CBF
- vascular tone
- vasomotion
- receptor functions
- calcium ion mobility

Figure 2 Summary of the effects of anesthesia on neurovascular coupling. The effects of anesthetics involve systemic physiology (i), neural processing (ii), vasoactive signal transmission (iii), and vascular responses (iv). Depending on the type and dose of anesthetic, the anesthesia differentially modifies the individual transfer functions of neural processing (f'_n), vasoactive signal transmission (g'_t), and vascular reactivity (h'_v). CBF, cerebral blood flow.

the temporal dynamics of vasodilation may vary between anesthetics. Finally, the quantitative coupling relationship of neurovascular responses is strongly influenced by anesthesia types and dosages. The fact that different anesthetics differentially modify the hemodynamic impulse response functions indicates that different anesthetics act specifically on the different cell populations that participate in the vasoactive pathways. In addition, this anesthesia interference may involve variations in baseline states, such as spontaneous neural activity, energy metabolism, and baseline CBF.

For *in-vivo* rodent somatosensory models, a large amount of neurovascular physiology and imaging data have been accumulated under α-chloralose anesthesia. Some findings might be specific to this anesthetic, such as the optimum stimulus frequency (Table 2) and low baseline CBF (Table 3). For repeated longitudinal experiments, isoflurane is recommended as an alternative agent because it provides easy control, good anesthesia recovery, and robust activity-induced vascular response that is comparable to that of α-chloralose in rat somatosensory models (Masamoto *et al*, 2007; Franceschini *et al*, 2010). Intravenous injection anesthesia (e.g., α-chloralose and medetomidine) carries concerns about the stability and reproducibility for long-term experiments (>3 hours), whereas urethane provides relatively long-term stability and balanced actions on multiple neurotransmitter receptors. Although some anesthetics, such as isoflurane, pentobarbital, and medetomidine, directly affect vascular physiology (i.e., dose-dependent vasodilation or vasoconstriction) independent of neural processing, the practical effects of these actions on neurovascular signal transmission remain relatively unknown. Because specific anesthetics may influence the specific cellular mechanisms of neurovascular elements, conducting multiple tests under different anesthesia conditions is recommended to ensure the exclusion of anesthesia confounds. This approach also helps determine the mechanisms of the generation of the signal in hemodynamic-based neuroimaging techniques.

Disclosure/conflict of interest

The authors declare no conflict of interest.

References

Akgören N, Dalgaard P, Lauritzen M (1996) Cerebral blood flow increases evoked by electrical stimulation of rat cerebellar cortex: relation to excitatory synaptic activity and nitric oxide synthesis. *Brain Res* 710:204–14

Altura BM, Altura BT, Carella A, Turlapaty PD, Weinberg J (1980) Vascular smooth muscle and general anesthetics. *Fed Proc* 39:1584–91

Ances BM, Zarahn E, Greenberg JH, Detre JA (2000) Coupling of neural activation to blood flow in the somatosensory cortex of rats is time-intensity separable, but not linear. *J Cereb Blood Flow Metab* 20:921–30

Arfors KE, Arturson G, Malmberg P (1971) Effect of prolonged chloralose anesthesia on acid-base balance and cardiovascular functions in dogs. *Acta Physiol Scand* 81:47–53

Attwell D, Buchan AM, Charpak S, Lauritzen M, Macvicar BA, Newman EA (2010) Glial and neuronal control of brain blood flow. *Nature* 468:232–43

Austin VC, Blamire AM, Allers KA, Sharp T, Styles P, Matthews PM, Sibson NR (2005) Confounding effects of anesthesia on functional activation in rodent brain: a study of halothane and alpha-chloralose anesthesia. *Neuroimage* 24:92–100

Ayata C, Dunn AK, Gursoy-OZdemir Y, Huang Z, Boas DA, Moskowitz MA (2004) Laser speckle flowmetry for the study of cerebrovascular physiology in normal and ischemic mouse cortex. *J Cereb Blood Flow Metab* 24:744–55

Berwick J, Johnston D, Jones M, Martindale J, Redgrave P, McLoughlin N, Schiessl I, Mayhew JE (2005) Neurovascular coupling investigated with two-dimensional optical imaging spectroscopy in rat whisker barrel cortex. *Eur J Neurosci* 22:1655–66

Berwick J, Martin C, Martindale J, Jones M, Johnston D, Zheng Y, Redgrave P, Mayhew J (2002) Hemodynamic response in the unanesthetized rat: intrinsic optical imaging and spectroscopy of the barrel cortex. *J Cereb Blood Flow Metab* 22:670–9

Bonvento G, Charbonné R, Corrèze JL, Borredon J, Seylaz J, Lacombe P (1994) Is alpha-chloralose plus halothane induction a suitable anesthetic regimen for cerebrovascular research? *Brain Res* 665:213–21

Boorman L, Kennerley AJ, Johnston D, Jones M, Zheng Y, Redgrave P, Berwick J (2010) Negative blood oxygen level dependence in the rat: a model for investigating the role of suppression in neurovascular coupling. *J Neurosci* 30:4285–94

Brinker G, Bock C, Busch E, Krep H, Hossmann KA, Hoehn-Berlage M (1999) Simultaneous recording of evoked potentials and T2*-weighted MR images during somatosensory stimulation of rat. *Magn Reson Med* 41:469–73

Brown CE, Boyd JD, Murphy TH (2010) Longitudinal *in vivo* imaging reveals balanced and branch-specific remodeling of mature cortical pyramidal dendritic arbors after stroke. *J Cereb Blood Flow Metab* 30:783–91

Chaigneau E, Oheim M, Audinat E, Charpak S (2003) Two-photon imaging of capillary blood flow in olfactory bulb glomeruli. *Proc Natl Acad Sci USA* 100:13081–6

Chaigneau E, Tiret P, Lecoq J, Ducros M, Knöpfel T, Charpak S (2007) The relationship between blood flow and neuronal activity in the rodent olfactory bulb. *J Neurosci* 27:6452–60

Chau PL (2010) New insights into the molecular mechanisms of general anaesthetics. *Br J Pharmacol* 161:288–307

Chen BR, Bouchard MB, McCaslin AF, Burgess SA, Hillman EM (2011) High-speed vascular dynamics of the hemodynamic response. *Neuroimage* 54:1021–30

Chen LM, Friedman RM, Ramsden BM, LaMotte RH, Roe AW (2001) Fine-scale organization of SI (area 3b) in the squirrel monkey revealed with intrinsic optical imaging. *J Neurophysiol* 86:3011–29

Chen Y, Aguirre AD, Ruvinskaya L, Devor A, Boas DA, Fujimoto JG (2009) Optical coherence tomography (OCT) reveals depth-resolved dynamics during functional brain activation. *J Neurosci Methods* 178:162–73

Colonnese MT, Phillips MA, Constantine-Paton M, Kaila K, Jasanoff A (2008) Development of hemodynamic responses and functional connectivity in rat somatosensory cortex. *Nat Neurosci* 11:72–9

Curtis DR, Lodge D (1977) Pentobarbitone enhancement of the inhibitory action of GABA. *Nature* 270:543–4

Devor A, Ulbert I, Dunn AK, Narayanan SN, Jones SR, Andermann ML, Boas DA, Dale AM (2005) Coupling of the cortical hemodynamic response to cortical and thalamic neuronal activity. *Proc Natl Acad Sci USA* 102:3822–7

Devor A, Tian P, Nishimura N, Teng IC, Hillman EM, Narayanan SN, Ulbert I, Boas DA, Kleinfeld D, Dale AM (2007) Suppressed neuronal activity and concurrent arteriolar vasoconstriction may explain negative blood oxygenation level-dependent signal. *J Neurosci* 27:4452–9

Dickinson R, Peterson BK, Banks P, Simillis C, Martin JC, Valenzuela CA, Maze M, Franks NP (2007) Competitive inhibition at the glycine site of the N-methyl-D-aspartate receptor by the anesthetics xenon and isoflurane: evidence from molecular modeling and electrophysiology. *Anesthesiology* 107:756–67

Dirnagl U, Kaplan B, Jacewicz M, Pulsinelli W (1989) Continuous measurement of cerebral cortical blood flow by laser-Doppler flowmetry in a rat stroke model. *J Cereb Blood Flow Metab* 9:589–96

Dombeck DA, Khabbaz AN, Collman F, Adelman TL, Tank DW (2007) Imaging large-scale neural activity with cellular resolution in awake, mobile mice. *Neuron* 56:43–57

Drew PJ, Shih AY, Kleinfeld D (2011) Fluctuating and sensory-induced vasodynamics in rodent cortex extend arteriole capacity. *Proc Natl Acad Sci USA* 108:8473–8

Du C, Pan Y (2011) Optical detection of brain function: simultaneous imaging of cerebral vascular response, tissue metabolism, and cellular activity *in vivo*. *Rev Neurosci* 22:695–709

Du C, Tully M, Volkow ND, Schiffer WK, Yu M, Luo Z, Koretsky AP, Benveniste H (2009) Differential effects of anesthetics on cocaine's pharmacokinetic and pharmacodynamic effects in brain. *Eur J Neurosci* 30:1565–75

Durduran T, Burnett MG, Yu G, Zhou C, Furuya D, Yodh AG, Detre JA, Greenberg JH (2004) Spatiotemporal quantification of cerebral blood flow during functional activation in rat somatosensory cortex using laser-speckle flowmetry. *J Cereb Blood Flow Metab* 24:518–25

Ebner TJ, Chen G (1995) Use of voltage-sensitive dyes and optical recordings in the central nervous system. *Prog Neurobiol* 46:463–506

Enager P, Piilgaard H, Offenhauser N, Kocharyan A, Fernandes P, Hamel E, Lauritzen M (2009) Pathway-specific variations in neurovascular and neurometabolic coupling in rat primary somatosensory cortex. *J Cereb Blood Flow Metab* 29:976–86

Fernández-Klett F, Offenhauser N, Dirnagl U, Priller J, Lindauer U (2010) Pericytes in capillaries are contractile *in vivo*, but arterioles mediate functional hyperemia in the mouse brain. *Proc Natl Acad Sci USA* 107: 22290–5

Field KJ, Lang CM (1988) Hazards of urethane (ethyl carbamate): a review of the literature. *Lab Anim* 22: 255–262

Field KJ, White WJ, Lang CM (1993) Anaesthetic effects of chloral hydrate, pentobarbitone and urethane in adult male rats. *Lab Anim* 27:258–69

Flynn N, Buljubasic N, Bosnjak ZJ, Kampine JP (1991) Cerebral vascular responses to anesthetics. *Adv Exp Med Biol* 301:237–46

Flynn NM, Buljubasic N, Bosnjak ZJ, Kampine JP (1992) Isoflurane produces endothelium-independent relaxation in canine middle cerebral arteries. *Anesthesiology* 76:461–7

Franceschini MA, Nissilä I, Wu W, Diamond SG, Bonmassar G, Boas DA (2008) Coupling between somatosensory evoked potentials and hemodynamic response in the rat. *Neuroimage* 41:189–203

Franceschini MA, Radhakrishnan H, Thakur K, Wu W, Ruvinskaya S, Carp S, Boas DA (2010) The effect of different anesthetics on neurovascular coupling. *Neuroimage* 51:1367–77

Franks NP (2008) General anaesthesia: from molecular targets to neuronal pathways of sleep and arousal. *Nat Rev Neurosci* 9:370–86

Fukuda M, Rajagopalan UM, Homma R, Matsumoto M, Nishizaki M, Tanifuji M (2005) Localization of activity-dependent changes in blood volume to submillimeter-scale functional domains in cat visual cortex. *Cereb Cortex* 15:823–33

Fuster J, Guiou M, Ardestani A, Cannestra A, Sheth S, Zhou YD, Toga A, Bodner M (2005) Near-infrared spectroscopy (NIRS) in cognitive neuroscience of the primate brain. *Neuroimage* 26:215–20

Ganjoo P, Farber NE, Hudetz A, Smith JJ, Samso E, Kampine JP, Schmeling WT (1998) *In vivo* effects of dexmedetomidine on laser-Doppler flow and pial arteriolar diameter. *Anesthesiology* 88:429–39

Garrett KM, Gan J (1998) Enhancement of gamma-aminobutyric acid A receptor activity by alpha-chloralose. *J Pharmacol Exp Ther* 285:680–6

Gerrits RJ, Raczynski C, Greene AS, Stein EA (2000) Regional cerebral blood flow responses to variable frequency whisker stimulation: an autoradiographic analysis. *Brain Res* 864:205–12

Gerrits RJ, Stein EA, Greene AS (1998) Blood flow increases linearly in rat somatosensory cortex with increased whisker movement frequency. *Brain Res* 783:151–7

Gerrits RJ, Stein EA, Greene AS (2001) Anesthesia alters NO-mediated functional hyperemia. *Brain Res* 907:20–6

Göbel W, Helmchen F (2007) *In vivo* calcium imaging of neural network function. *Physiology (Bethesda)* 22: 358–365

Gordon EL, Meno JR, Ngai AC, Lam AM, Winn HR (1995) Anesthetic-dependent pial arteriolar response to ethanol. *J Neurosurg* 83:875–7

Gu W, Jiang W, Wester P (2003) Real-time cortical cerebral blood flow follow-up in conscious, freely moving rats by laser Doppler flowmetry. *Methods* 30:172–7

Gyngell ML, Bock C, Schmitz B, Hoehn-Berlage M, Hossmann KA (1996) Variation of functional MRI signal in response to frequency of somatosensory stimulation in alpha-chloralose anesthetized rats. *Magn Reson Med* 36:13–5

Hara K, Harris RA (2002) The anesthetic mechanism of urethane: the effects on neurotransmitter-gated ion channels. *Anesth Analg* 94:313–8

Harris S, Jones M, Zheng Y, Berwick J (2010) Does neural input or processing play a greater role in the magnitude of neuroimaging signals? *Front Neuroenergetics* 2:1–7

Hayton SM, Kriss A, Muller DP (1999) Comparison of the effects of four anaesthetic agents on somatosensory evoked potentials in the rat. *Lab Anim* 33:243–51

Helmchen F (2002) Miniaturization of fluorescence microscopes using fibre optics. *Exp Physiol* 87:737–45

Hemmings Jr HC (2009) Sodium channels and the synaptic mechanisms of inhaled anaesthetics. *Br J Anaesth* 103:61–9

Hentschke H, Schwarz C, Antkowiak B (2005) Neocortex is the major target of sedative concentrations of volatile anaesthetics: strong depression of firing rates and increase of GABAA receptor-mediated inhibition. *Eur J Neurosci* 21:93–102

Hillman EM, Devor A, Bouchard MB, Dunn AK, Krauss GW, Skoch J, Bacskai BJ, Dale AM, Boas DA (2007) Depth-resolved optical imaging and microscopy of vascular compartment dynamics during somatosensory stimulation. *Neuroimage* 35:89–104

Hirano Y, Stefanovic B, Silva AC (2011) Spatiotemporal evolution of the functional magnetic resonance imaging response to ultrashort stimuli. *J Neurosci* 31:1440–7

Homma R, Baker BJ, Jin L, Garaschuk O, Konnerth A, Cohen LB, Zecevic D (2009) Wide-field and two-photon imaging of brain activity with voltage- and calcium-sensitive dyes. *Philos Trans R Soc Lond B Biol Sci* 364:2453–67

Huttunen JK, Gröhn O, Penttonen M (2008) Coupling between simultaneously recorded BOLD response and neuronal activity in the rat somatosensory cortex. *Neuroimage* 39:775–85

Hyder F, Kennan RP, Kida I, Mason GF, Behar KL, Rothman D (2000) Dependence of oxygen delivery on blood flow in rat brain: a 7 tesla nuclear magnetic resonance study. *J Cereb Blood Flow Metab* 20:485–98

Hyder F, Rothman DL, Shulman RG (2002) Total neuroenergetics support localized brain activity: implications for the interpretation of fMRI. *Proc Natl Acad Sci USA* 99:10771–6

Iadecola C (2004) Neurovascular regulation in the normal brain and in Alzheimer's disease. *Nat Rev Neurosci* 5:347–60

Iida H, Ohata H, Iida M, Watanabe Y, Dohi S (1998) Isoflurane and sevoflurane induce vasodilation of cerebral vessels via ATP-sensitive K+ channel activation. *Anesthesiology* 89:954–60

Jin T, Kim SG (2008) Cortical layer-dependent dynamic blood oxygenation, cerebral blood flow and cerebral blood volume responses during visual stimulation. *Neuroimage* 43:1–9

Jones M, Berwick J, Johnston D, Mayhew J (2001) Concurrent optical imaging spectroscopy and laser-Doppler flowmetry: the relationship between blood flow, oxygenation, and volume in rodent barrel cortex. *Neuroimage* 13:1002–15

Jukovskaya N, Tiret P, Lecoq J, Charpak S (2011) What does local functional hyperemia tell about local neuronal activation? *J Neurosci* 31:1579–82

Kannurpatti SS, Biswal BB (2006) Spatial extent of CBF response during whisker stimulation using trial averaged laser Doppler imaging. *Brain Res* 1089:135–42

Kannurpatti SS, Biswal BB (2011) Frequency tuning in the rat whisker barrel cortex revealed through RBC flux maps. *Brain Res* 1417:16–26

Keilholz SD, Silva AC, Raman M, Merkle H, Koretsky AP (2004) Functional MRI of the rodent somatosensory pathway using multislice echo planar imaging. *Magn Reson Med* 52:89–99

Keller CJ, Cash SS, Narayanan S, Wang C, Kuzniecky R, Carlson C, Devinsky O, Thesen T, Doyle W, Sassaroli A, Boas DA, Ulbert I, Halgren E (2009) Intracranial microprobe for evaluating neuro-hemodynamic coupling in unanesthetized human neocortex. *J Neurosci Methods* 179:208–18

Khananashvili YA, Demidova AA (2002) Dynamics of the development of microvascular reactions in the projection zones of the somatosensory cortex of the brain in rats. *Neurosci Behav Physiol* 32:435–42

Kim T, Hendrich KS, Masamoto K, Kim SG (2007) Arterial versus total blood volume changes during neural activity-induced cerebral blood flow change: implication for BOLD fMRI. *J Cereb Blood Flow Metab* 27: 1235–1247

Kim T, Masamoto K, Fukuda M, Vazquez A, Kim SG (2010) Frequency-dependent neural activity, CBF, and BOLD fMRI to somatosensory stimuli in isoflurane-anesthetized rats. *Neuroimage* 52:224–33

Kleinfeld D, Blinder P, Drew PJ, Driscoll JD, Muller A, Tsai PS, Shih AY (2011) A guide to delineate the logic of neurovascular signaling in the brain. *Front Neuroenergetics* 3:1–9

Kleinfeld D, Mitra PP, Helmchen F, Denk W (1998) Fluctuations and stimulus-induced changes in blood flow observed in individual capillaries in layers 2 through 4 of rat neocortex. *Proc Natl Acad Sci USA* 95:15741–6

Krautwald K, Angenstein F (2012) Low frequency stimulation of the perforant pathway generates anesthesia-specific variations in neural activity and BOLD responses in the rat dentate gyrus. *J Cereb Blood Flow Metab* 32:291–305

Kuschinsky W, Suda S, Sokoloff L (1985) Influence of gamma-hydroxybutyrate on the relationship between local cerebral glucose utilization and local cerebral blood flow in the rat brain. *J Cereb Blood Flow Metab* 5: 58–64

Lahti KM, Ferris CF, Li F, Sotak CH, King JA (1998) Imaging brain activity in conscious animals using functional MRI. *J Neurosci Methods* 82:75–83

Lahti KM, Ferris CF, Li F, Sotak CH, King JA (1999) Comparison of evoked cortical activity in conscious and propofol-anesthetized rats using functional MRI. *Magn Reson Med* 41:412–6

Lauritzen M (2001) Relationship of spikes, synaptic activity, and local changes of cerebral blood flow. *J Cereb Blood Flow Metab* 21:1367–83

Lecrux C, Toussay X, Kocharyan A, Fernandes P, Neupane S, Lévesque M, Plaisier F, Shmuel A, Cauli B, Hamel E (2011) Pyramidal neurons are "neurogenic hubs" in the neurovascular coupling response to whisker stimulation. *J Neurosci* 31:9836–47

Lee JG, Hudetz AG, Smith JJ, Hillard CJ, Bosnjak ZJ, Kampine JP (1994) The effects of halothane and isoflurane on cerebrocortical microcirculation and autoregulation as assessed by laser-Doppler flowmetry. *Anesth Analg* 79:58–65

Lee JG, Smith JJ, Hudetz AG, Hillard CJ, Bosnjak ZJ, Kampine JP (1995) Laser-Doppler measurement of the effects of halothane and isoflurane on the cerebrovascular CO2 response in the rat. *Anesth Analg* 80:696–702

Lee SP, Duong TQ, Yang G, Iadecola C, Kim SG (2001) Relative changes of cerebral arterial and venous blood volumes during increased cerebral blood flow: implications for BOLD fMRI. *Magn Reson Med* 45:791–800

Leniger-Follert E, Hossmann KA (1979) Simultaneous measurements of microflow and evoked potentials in the somatomotor cortex of the cat brain during specific sensory activation. *Pflugers Arch* 380:85–9

Lenz C, Rebel A, van Ackern K, Kuschinsky W, Waschke KF (1998) Local cerebral blood flow, local cerebral glucose utilization, and flow-metabolism coupling during sevoflurane versus isoflurane anesthesia in rats. *Anesthesiology* 89:1480–8

Lincoln DW (1969) Correlation of unit activity in the hypothalamus with EEG patterns associated with the sleep cycle. *Exp Neurol* 24:1–18

Lindauer U, Villringer A, Dirnagl U (1993) Characterization of CBF response to somatosensory stimulation: model and influence of anesthetics. *Am J Physiol* 264:H1223–8

Logothetis NK, Pauls J, Augath M, Trinath T, Oeltermann A (2001) Neurophysiological investigation of the basis of the fMRI signal. *Nature* 412:150–7

Lukasik VM, Gillies RJ (2003) Animal anaesthesia for *in vivo* magnetic resonance. *NMR Biomed* 16:459–67

Maekawa T, Tommasino C, Shapiro HM, Keifer-Goodman J, Kohlenberger RW (1986) Local cerebral blood flow and glucose utilization during isoflurane anesthesia in the rat. *Anesthesiology* 65:144–51

Maggi CA, Meli A (1986) Suitability of urethane anesthesia for physiopharmacological investigations in various systems. Part 1: General considerations. *Experientia* 42:109–14

Maheswari RU, Takaoka H, Kadono H, Homma R, Tanifuji M (2003) Novel functional imaging technique from brain surface with optical coherence tomography enabling visualization of depth resolved functional structure *in vivo*. *J Neurosci Methods* 124:83–92

Mantz J, Cordier J, Giaume C (1993) Effects of general anesthetics on intercellular communications mediated by gap junctions between astrocytes in primary culture. *Anesthesiology* 78:892–901

Martin C, Berwick J, Johnston D, Zheng Y, Martindale J, Port M, Redgrave P, Mayhew J (2002) Optical imaging spectroscopy in the unanaesthetised rat. *J Neurosci Methods* 120:25–34

Martin C, Martindale J, Berwick J, Mayhew J (2006) Investigating neural- hemodynamic coupling and the hemodynamic response function in the awake rat. *Neuroimage* 32:33–48

Martindale J, Mayhew J, Berwick J, Jones M, Martin C, Johnston D, Redgrave P, Zheng Y (2003) The hemodynamic impulse response to a single neural event. *J Cereb Blood Flow Metab* 23:546–55

Masamoto K, Fukuda M, Vazquez A, Kim SG (2009) Dose-dependent effect of isoflurane on neurovascular coupling in rat cerebral cortex. *Eur J Neurosci* 30:242–50

Masamoto K, Kim T, Fukuda M, Wang P, Kim SG (2007) Relationship between neural, vascular, and BOLD signals in isoflurane-anesthetized rat somatosensory cortex. *Cereb Cortex* 17:942–50

Masamoto K, Obata T, Kanno I (2010**a**) Cerebrovascular dynamics in response to neural stimulation. *Hirosaki Med J* 61:S181–6

Masamoto K, Obata T, Kanno I (2010**b**) Intracortical microcirculatory change induced by anesthesia in rat somatosensory cortex. *Adv Exp Med Biol* 662:57–61

Matsuura T, Fujita H, Kashikura K, Kanno I (2000) Evoked local cerebral blood flow induced by somatosensory stimulation is proportional to the baseline flow. *Neurosci Res* 38:341–8

Matsuura T, Fujita H, Seki C, Kashikura K, Kanno I (1999) Hemodynamics evoked by microelectrical direct stimulation in rat somatosensory cortex. *Comp Biochem Physiol A Mol Integr Physiol* 124:47–52

Matsuura T, Kanno I (2001) Quantitative and temporal relationship between local cerebral blood flow and neuronal activation induced by somatosensory stimulation in rats. *Neurosci Res* 40:281–90

Minchin MC (1981) The effect of anaesthetics on the uptake and release of gamma-aminobutyrate and D-aspartate in rat brain slices. *Br J Pharmacol* 73:681–9

Miyazaki H, Nakamura Y, Arai T, Kataoka K (1997) Increase of glutamate uptake in astrocytes: a possible mechanism of action of volatile anesthetics. *Anesthesiology* 86: 1359–66

Moskalenko YE, Dowling JL, Liu D, Rovainen CM, Semernia VN, Woolsey TA (1996) LCBF changes in rat somatosensory cortex during whisker stimulation monitored by dynamic H2 clearance. *Int J Psychophysiol* 21: 45–59

Nakamura K, Terasako K, Toda H, Miyawaki I, Kakuyama M, Nishiwada M, Hatano Y, Mori K (1994) Mechanisms of inhibition of endothelium-dependent relaxation by halothane, isoflurane, and sevoflurane. *Can J Anaesth* 41:340–6

Nakao Y, Itoh Y, Kuang TY, Cook M, Jehle J, Sokoloff L (2001) Effects of anesthesia on functional activation of cerebral blood flow and metabolism. *Proc Natl Acad Sci USA* 98:7593–8

Ngai AC, Jolley MA, D'Ambrosio R, Meno JR, Winn HR (1999) Frequency-dependent changes in cerebral blood flow and evoked potentials during somatosensory stimulation in the rat. *Brain Res* 837:221–8

Nicoll RA (1978) Pentobarbital: differential postsynaptic actions on sympathetic ganglion cells. *Science* 199: 451–2

Nielsen NA, Lauritzen M (2001) Coupling and uncoupling of activity-dependent increases of neuronal activity and blood flow in rat somatosensory cortex. *J Physiol* 533:773–85

Obrenovitch TP, Chen S, Farkas E (2009) Simultaneous, live imaging of cortical spreading depression and associated cerebral blood flow changes, by combining voltage-sensitive dye and laser speckle contrast methods. *Neuroimage* 45:68–74

Obrig H, Villringer A (2003) Beyond the visible–imaging the human brain with light. *J Cereb Blood Flow Metab* 23:1–18

Ogawa S, Lee TM, Stepnoski R, Chen W, Zhu XH, Ugurbil K (2000) An approach to probe some neural systems interaction by functional MRI at neural time scale down to milliseconds. *Proc Natl Acad Sci USA* 97:11026–31

Ogura K, Takayasu M, Dacey Jr RG (1991) Differential effects of pentobarbital on intracerebral arterioles and venules of rats *in vitro*. *Neurosurgery* 28:537–41

Otsuka T, Wei L, Acuff VR, Shimizu A, Pettigrew KD, Patlak CS, Fenstermacher JD (1991) Variation in local cerebral blood flow response to high-dose pentobarbital sodium in the rat. *Am J Physiol* 261:H110–20

Ou W, Nissilä I, Radhakrishnan H, Boas DA, Hämäläinen MS, Franceschini MA (2009) Study of neurovascular coupling in humans via simultaneous magnetoencephalography and diffuse optical imaging acquisition. *Neuroimage* 46:624–32

Pawela CP, Biswal BB, Hudetz AG, Schulte ML, Li R, Jones SR, Cho YR, Matloub HS, Hyde JS (2009) A protocol for use of medetomidine anesthesia in rats for extended studies using task-induced BOLD contrast and resting-state functional connectivity. *Neuroimage* 46:1137–47

Peeters RR, Tindemans I, De Schutter E, Van der Linden A (2001) Comparing BOLD fMRI signal changes in the awake and anesthetized rat during electrical forepaw stimulation. *Magn Reson Imaging* 19:821–6

Reinert H (1964) Urethane hyperclycaemia and hypothalamic activation. *Nature* 204:889–91

Reinert KC, Gao W, Chen G, Ebner TJ (2007) Flavoprotein autofluorescence imaging in the cerebellar cortex *in vivo*. *J Neurosci Res* 85:3221–32

Rosengarten B, Kaps M (2010) A simultaneous EEG and transcranial Doppler technique to investigate the neurovascular coupling in the human visual cortex. *Cerebrovasc Dis* 29:211–6

Sandman CA, O'Halloran JP, Isenhart R (1984) Is there an evoked vascular response? *Science* 224:1355–7

Sándor P, Nyáry I, Reivich M, Kovách AG (1977) Comparative effects of chloralose anesthesia and Sernylan analgesia on cerebral blood flow, CO2 responsiveness, and brain metabolism in the baboon. *Stroke* 8:432–6

Sandstrom DJ (2004) Isoflurane depresses glutamate release by reducing neuronal excitability at the Drosophila neuromuscular junction. *J Physiol* 558:489–502

Sanganahalli BG, Herman P, Hyder F (2008) Frequency-dependent tactile responses in rat brain measured by functional MRI. *NMR Biomed* 21:410–6

Schregardus DS, Pieneman AW, Ter Maat A, Jansen RF, Brouwer TJ, Gahr ML (2006) A lightweight telemetry system for recording neuronal activity in freely behaving small animals. *J Neurosci Methods* 155:62–71

Schulte ML, Hudetz AG (2006) Functional hyperemic response in the rat visual cortex under halothane anesthesia. *Neurosci Lett* 394:63–8

Sebel PS, Ingram DA, Flynn PJ, Rutherfoord CF, Rogers H (1986) Evoked potentials during isoflurane anaesthesia. *Br J Anaesth* 58:580–5

Seylaz J, Charbonné R, Nanri K, Von Euw D, Borredon J, Kacem K, Méric P, Pinard E (1999) Dynamic *in vivo* measurement of erythrocyte velocity and flow in capillaries and of microvessel diameter in the rat brain by confocal laser microscopy. *J Cereb Blood Flow Metab* 19:863–70

Sheth S, Nemoto M, Guiou M, Walker M, Pouratian N, Toga AW (2003) Evaluation of coupling between optical intrinsic signals and neuronal activity in rat somatosensory cortex. *Neuroimage* 19:884–94

Sheth SA, Nemoto M, Guiou M, Walker M, Pouratian N, Toga AW (2004) Linear and nonlinear relationships between neuronal activity, oxygen metabolism, and hemodynamic responses. *Neuron* 42:347–55

Sheth SA, Nemoto M, Guiou MW, Walker MA, Toga AW (2005) Spatiotemporal evolution of functional hemodynamic changes and their relationship to neuronal activity. *J Cereb Blood Flow Metab* 25:830–41

Shibuki K, Hishida R, Murakami H, Kudoh M, Kawaguchi T, Watanabe M, Watanabe S, Kouuchi T, Tanaka R (2003) Dynamic imaging of somatosensory cortical activity in the rat visualized by flavoprotein autofluorescence. *J Physiol* 549:919–27

Shtoyerman E, Arieli A, Slovin H, Vanzetta I, Grinvald A (2000) Long-term optical imaging and spectroscopy reveal mechanisms underlying the intrinsic signal and stability of cortical maps in V1 of behaving monkeys. *J Neurosci* 20:8111–21

Shulman RG, Rothman DL, Hyder F (1999) Stimulated changes in localized cerebral energy consumption under anesthesia. *Proc Natl Acad Sci USA* 96:3245–50

Sicard K, Shen Q, Brevard ME, Sullivan R, Ferris CF, King JA, Duong TQ (2003) Regional cerebral blood flow and BOLD responses in conscious and anesthetized rats under basal and hypercapnic conditions: implications for functional MRI studies. *J Cereb Blood Flow Metab* 23:472–81

Silva AC, Koretsky AP (2002) Laminar specificity of functional MRI onset times during somatosensory stimulation in rat. *Proc Natl Acad Sci USA* 99:15182–7

Silva AC, Lee SP, Yang G, Iadecola C, Kim SG (1999) Simultaneous blood Oxygenation level-dependent and cerebral blood flow functional magnetic resonance imaging during forepaw stimulation in the rat. *J Cereb Blood Flow Metab* 19:871–9

Silva AC, Lee SP, Iadecola C, Kim SG (2000) Early temporal characteristics of cerebral blood flow and deoxyhemoglobin changes during somatosensory stimulation. *J Cereb Blood Flow Metab* 20:201–6

Silverman J, Muir III WW (1993) A review of laboratory animal anesthesia with chloral hydrate and chloralose. *Lab Anim Sci* 43:210–6

Sinclair MD (2003) A review of the physiological effects of alpha2-agonists related to the clinical use of medetomidine in small animal practice. *Can Vet J* 44:885–97

Smith AJ, Blumenfeld H, Behar KL, Rothman DL, Shulman RG, Hyder F (2002) Cerebral energetics and spiking frequency: the neurophysiological basis of fMRI. *Proc Natl Acad Sci USA* 99:10765–70

Sun X, Wang Y, Chen S, Luo W, Li P, Luo Q (2011) Simultaneous monitoring of intracellular pH changes and hemodynamic response during cortical spreading depression by fluorescence-corrected multimodal optical imaging. *Neuroimage* 57:873–84

Takano T, Tian GF, Peng W, Lou N, Libionka W, Han X, Nedergaard M (2006) Astrocyte-mediated control of cerebral blood flow. *Nat Neurosci* 9:260–7

Takashima I, Kajiwara R, Iijima T (2001) Voltage-sensitive dye versus intrinsic signal optical imaging: comparison of optically determined functional maps from rat barrel cortex. *Neuroreport* 12:2889–94

Takuwa H, Autio J, Nakayama H, Matsuura T, Obata T, Okada E, Masamoto K, Kanno I (2011) Reproducibility and variance of a stimulation-induced hemodynamic response in barrel cortex of awake behaving mice. *Brain Res* 1369:103–11

Tanaka K, Kawano T, Tsutsumi YM, Kinoshita M, Kakuta N, Hirose K, Kimura M, Oshita S (2011) Differential effects of propofol and isoflurane on glucose utilization and insulin secretion. *Life Sci* 88:96–103

Tétrault S, Chever O, Sik A, Amzica F (2008) Opening of the blood-brain barrier during isoflurane anaesthesia. *Eur J Neurosci* 28:1330–41

Tian P, Teng IC, May LD, Kurz R, Lu K, Scadeng M, Hillman EM, De Crespigny AJ, D'Arceuil HE, Mandeville JB, Marota JJ, Rosen BR, Liu TT, Boas DA, Buxton RB, Dale AM, Devor A (2010) Cortical depth-specific microvascular dilation underlies laminar differences in blood oxygenation level-dependent functional MRI signal. *Proc Natl Acad Sci USA* 107:15246–51

Toda H, Nakamura K, Hatano Y, Nishiwada M, Kakuyama M, Mori K (1992) Halothane and isoflurane inhibit endothelium-dependent relaxation elicited by acetylcholine. *Anesth Analg* 75:198–203

Tomita Y, Kubis N, Calando Y, Tran Dinh A, Méric P, Seylaz J, Pinard E (2005) Long-term *in vivo* investigation of mouse cerebral microcirculation by fluorescence confocal microscopy in the area of focal ischemia. *J Cereb Blood Flow Metab* 25:858–67

Tsuji T, Chiba S (1987) Mechanism of vascular responsiveness to barbiturates in isolated and perfused canine basilar arteries. *Neurosurgery* 21:161–6

Tung A, Herrera S, Fornal CA, Jacobs BL (2008) The effect of prolonged anesthesia with isoflurane, propofol, dexmedetomidine, or ketamine on neural cell proliferation in the adult rat. *Anesth Analg* 106:1772–7

Ueki M, Mies G, Hossmann KA (1992) Effect of alpha-chloralose, halothane, pentobarbital and nitrous oxide anesthesia on metabolic coupling in somatosensory cortex of rat. *Acta Anaesthesiol Scand* 36:318–22

Van Aken H, van Hemelrijck J (1991) Influence of anesthesia on cerebral blood flow and cerebral metabolism: an overview. *Agressologie* 32:303–6

Van Camp N, Verhoye M, Van der Linden A (2006) Stimulation of the rat somatosensory cortex at different frequencies and pulse widths. *NMR Biomed* 19:10–7

Vanzetta I, Grinvald A (2008) Coupling between neuronal activity and microcirculation: implications for functional brain imaging. *HFSP J* 2:79–98

Villringer A, Dirnagl U (1995) Coupling of brain activity and cerebral blood flow: basis of functional neuroimaging. *Cerebrovasc Brain Metab Rev* 7:240–76

Villringer A, Them A, Lindauer U, Einhäupl K, Dirnagl U (1994) Capillary perfusion of the rat brain cortex. An *in vivo* confocal microscopy study. *Circ Res* 75:55–62

Violet JM, Downie DL, Nakisa RC, Lieb WR, Franks NP (1997) Differential sensitivities of mammalian neuronal and muscle nicotinic acetylcholine receptors to general anesthetics. *Anesthesiology* 86:866–74

Vogel J, Kuschinsky W (1996) Decreased heterogeneity of capillary plasma flow in the rat whisker-barrel cortex during functional hyperemia. *J Cereb Blood Flow Metab* 16:1300–6

Wang K, Zheng C, Wu C, Gao M, Liu Q, Yang K, Ellsworth K, Xu L, Wu J (2008) alpha-Chloralose diminishes gamma oscillations in rat hippocampal slices. *Neurosci Lett* 441:66–71

Weber B, Burger C, Wyss MT, von Schulthess GK, Scheffold F, Buck A (2004) Optical imaging of the spatiotemporal dynamics of cerebral blood flow and oxidative metabolism in the rat barrel cortex. *Eur J Neurosci* 20:2664–70

Weber R, Ramos-Cabrer P, Wiedermann D, van Camp N, Hoehn M (2006) A fully noninvasive and robust experimental protocol for longitudinal fMRI studies in the rat. *Neuroimage* 29:1303–10

Wei L, Otsuka T, Acuff V, Bereczki D, Pettigrew K, Patlak C, Fenstermacher J (1993) The velocities of red cell and plasma flows through parenchymal microvessels of rat brain are decreased by pentobarbital. *J Cereb Blood Flow Metab* 13:487–97

Williams KA, Magnuson M, Majeed W, LaConte SM, Peltier SJ, Hu X, Keilholz SD (2010) Comparison of alpha-chloralose, medetomidine and isoflurane anesthesia for functional connectivity mapping in the rat. *Magn Reson Imaging* 28:995–1003

Wu XS, Sun JY, Evers AS, Crowder M, Wu LG (2004) Isoflurane inhibits transmitter release and the presynaptic action potential. *Anesthesiology* 100:663–670

Zhao F, Zhao T, Zhou L, Wu Q, Hu X (2008) BOLD study of stimulation-induced neural activity and resting-state connectivity in medetomidine-sedated rat. *Neuroimage* 39:248–60

3D Analysis of Intracortical Microvasculature during Chronic Hypoxia in Mouse Brains

Kouichi Yoshihara[1], Hiroyuki Takuwa[2], Iwao Kanno[2], Shinpei Okawa[1], Yukio Yamada[1] and Kazuto Masamoto[2,3]

[1]Department of Mechanical Engineering and Intelligent Systems, University of Electro-Communications, Japan, [2]Molecular Imaging Center, National Institute of Radiological Sciences, Japan, [3]Center for Frontier Science and Engineering, University of Electro-Communications, Japan

Abstract The purpose of this study is to determine when and where the brain microvasculature changes its network in response to chronic hypoxia. To identify the hypoxia-induced structural adaptation, we longitudinally imaged cortical microvasculature at the same location within a mouse somatosensory cortex with two-photon microscopy repeatedly for up to one month during continuous exposure to hypoxia (either 8% or 10% oxygen conditions). The two-photon microscopy approach made it possible to track a 3D pathway from a cortical surface arteriole to a venule up to a depth of 0.8 mm from the cortical surface. The network pathway was then divided into individual vessel segments at the branches, and their diameters and lengths were measured. We observed 3 to 11 vessel segments between the penetrating arteriole and the emerging vein over the depths of 20 to 460 μm within the 3D reconstructed image (0.46 x 0.46 x 0.80 mm^3). The average length of the individual capillaries (< 7 μm in diameter) was 67 ± 46 μm, which was not influenced by hypoxia. In contrast, 1.4 ± 0.3 and 1.2 ± 0.2 fold increases of the capillary diameter were observed 1 week after exposure to 8% and 10% hypoxia, respectively. At 3 weeks from the exposure, the capillary diameter reached 8.5 ± 1.9 μm and 6.7 ± 1.8 μm in 8% and 10% hypoxic conditions, respectively, which accounted for the 1.8 ± 0.5 and 1.4 ± 0.3 fold increases relative to those of the prehypoxic condition. The vasodilation of penetrating arterioles (1.4 ± 0.2 and 1.2 ± 0.2 fold increases) and emerging veins (1.3 ± 0.2 and 1.3 ± 0.2 fold increases) showed relatively small diameter changes compared with the parenchymal capillaries. These findings indicate that parenchymal capillaries are the major site responding to the oxygen environment during chronic hypoxia.

1 Introduction

The brain is known to be an organ vulnerable to a lack of oxygen. Only 2 to 3 minutes without an adequate oxygen supply leads to irreversible damage of central

nervous system (CNS) functions. To maintain an adequate supply, the brain vasculature is well organized to allow the diffusion of oxygen to every region of the tissue[1]. Previous studies have shown that the density of brain microvessels adaptively increased in response to chronic hypoxia[2,3]. Angiogenesis and degeneration of the microvasculature were also reported in response to a progress of brain tumors and Alzheimer's disease, respectively[4,5]. These studies strongly indicate that close interaction exists between brain microvasculature and tissue activity to maintain an adequate supply of oxygen. However, the mechanism that regulates the brain microvasculature and its effect on tissue oxygen homeostasis remains mostly unknown.

Because one of the reasons for the lack of knowledge about the structural adaptations of brain microvasculature is a lack of longitudinal studies at the capillary network scale, here, we longitudinally tracked the spatial and temporal adaptation of the microvasculature during chronic hypoxia in a mouse somatosensory cortex with two-photon microscopy. The same three-dimensional (3D) microvasculature was imaged every week for up to one month during continuous exposure to hypoxia (at either 8% or 10% oxygen). Two-photon microscopy is based on the principle of nonlinear optics[6,7,8]. In addition, two-photon microscopy allows excitation with near-infrared light, which has the advantage of providing a long penetration depth in biological tissues[9]. In the present study, volume images of the cortical microvasculature were captured up to a depth of 0.8 mm from the cortical surface with a step size of 0.005 mm and reconstructed with 3D rendering. The 3D pathways of the parenchymal microvasculature were identified and divided into individual segments at the branches. The diameters and lengths of the segments were measured, and their temporal changes were longitudinally traced over the periods of the measurements. Finally, the surface areas and volumes of the vessel segments were calculated to evaluate the adaptation of the microvasculature.

2 Materials and Methods

2.1 Image Analysis

The 3D image (field of view: $0.46\times0.46\times0.80$ mm^3) consists of approximately 160 2D images in the x-y plane parallel to the brain surface with a depth step of 5 μm, and each 2D image has 1024×1024 pixels with an individual pixel size of 0.45 μm. The image analysis performed in each step is described below.

(i) Identification of parenchymal arteriovenous pathway

One target pathway between a surface artery and a vein through parenchymal microvasculature was identified within the reconstructed image (Figs. 1a,b), by

tracking all branches from the artery to the vein including penetrating arterioles, parenchymal capillaries (< 7 μm in diameter), and emerging veins.

(ii) Segmentation of vessels

The vessel segments in the pathway were sequentially numbered (Fig. 1c). One vessel segment was defined as the vessel having two-branches at both ends. The sequential numbers were assigned, beginning from the penetrating artery and ending with the emerging vein.

(iii) Measurement of the length of a vessel segment

The vessel length was measured as the distance from one end to the other end along the centerline of the vessel segment. Several measurement points were manually placed on the centerline to account for the curvature of the vessel. By summing all the distances between the neighboring two measuring points, the vessel length was obtained.

(iv) Measurement of the vessel diameter

The vessel diameter was measured as the average of the diameters at 10 different positions in the vessel segment. Because the intensity differences (i.e., contrast) in the images were sufficient to discriminate the vessel edges relative to the tissue, it was not difficult to manually assign the edges of the vessels to measure the vessel diameters (Fig. 1d).

(v) Calculation of the vessel surface area and volume

The surface areas and volumes of each vessel segment were calculated from the measured diameters and lengths by assuming that each vessel segment was approximated as a cylinder.

2.2. Animal experiments

All experimental protocols were approved by the Institutional Animal Care and Use Committee of the National Institute of Radiological Sciences and the University of Electro-Communications, and the experiments were conducted by following the approved protocols. Ten male C57BL/6J mice (21–23 g) were randomly divided into two groups: one for the 8% oxygen experiment (n=5) and the other for the 10% oxygen experiment (n=5). A custom-made fixation device was fixed to the animal's head for two-photon microscopy imaging[10]. At 2 weeks post-operation, the experiments with hypoxic exposure initiated. During the imaging experiments, the mice were anesthetized with isoflurane (1%) in a mixture of air and oxygen gas, and their rectal temperature was maintained at 37±1°C. Sulforhodamine 101 (SR101) dissolved in saline (5 mM) was intraperitoneally injected into the animal (8 mL/kg) for labeling blood plasma, and cortical vasculature was imaged with a two-photon microscope (TCS SP5MP, Leica Microsystems, Germany) equipped with a Ti:Sapphire laser (MaiTai HP, Spectra-Physics, CA). The excitation wavelength was 900 nm (average power 2.0 W output), and the emission signal was detected through a bandpass filter (610/75 nm).

At day 0 (start of exposure to hypoxia), a reference image of the cortical surface vasculature was obtained with reflection acquisition mode excited at 633 nm with a low magnification object lens (field of view: 3.6×3.6 mm^2). The cortical arteries and veins were distinguished in the reflection image; the arteries and veins exhibited different light intensities because of their different light absorption characteristics[9]. Because the pattern of the cortical surface vessels was preserved over the period of the longitudinal experiments, the reference image was used to identify the measurement locations at different imaging experiments. Except while undergoing imaging, the animals were kept in either an 8% or 10% oxygen room in which the oxygen level was monitored with an oxygen sensor. The imaging experiments were repeatedly performed on days 0, 7, 14, 21, and 31 after exposure to hypoxia. Because 3 out of 5 animals were dead after 3 weeks in the 8% oxygen experiment, the analytical results were only compared for the first 3 weeks of measurements. Data were represented as mean ± standard deviation.

3. Results and Discussion

Reconstructed 3D images of cortical microvasculature are represented in Fig. 2. The images show the apparently same 3D structures over the period of one month during continuous exposure to hypoxia. The 3D pathways were identified from penetrating arteriole (A) to emerging vein (V) through parenchymal capillaries (C), which had 5 to 13 branches between the surface artery and the vein over depths of 20 to 460 μm within the image. The total length from the beginning of a penetrating arteriole to the end point of the emerging vein was 703 ± 278 μm (311 -1221 μm, n=30 networks), which was unchanged during chronic hypoxia over 3 weeks (Table 1). In contrast, the parenchymal capillary diameter was predominantly increased by 1.4 ± 0.3 and 1.2 ± 0.2 fold at 1 week after continuous exposure to 8% and 10% oxygen, respectively (Table 1). The vasodilation of parenchymal capillaries continued over 3 weeks: 1.8 ± 0.5 and 1.4 ± 0.3 fold relative to that of the prehypoxic condition. This increase was significantly higher than both the penetrating arterioles (1.4 ± 0.2 times) and emerging veins (1.3 ± 0.2 times) under the 8% oxygen condition but not the 10% oxygen condition (1.2 ± 0.2 fold for arterioles and 1.3 ± 0.2 fold for veins). Consequently, the vessel surface area increased by 1.5 ± 0.4, 1.8 ± 0.7, and 1.2 ± 0.3 fold for arterioles, capillaries, and veins after 3 weeks under 8% oxygen exposure and by 1.2 ± 0.3, 1.4 ± 0.5, and 1.3 ± 0.3 fold for 10% oxygen, respectively. In addition, the vessel volume was 2.1 ± 0.9, 3.5 ± 2.5, and 1.7 ± 0.6 times larger for 8% oxygen and 1.6 ± 0.5, 2.1 ± 1.6, and 1.6 ± 0.6 times larger for 10% oxygen. These results show that depending on the level of hypoxia, vascular restructuring was induced for different vessel types. In particular, the lower oxygen level (8%) caused a predominant increase in the parenchymal capillary volumes, indicating that several mechanisms may be participating in the hypoxia-induced restructuring of cortical microvasculature. Future studies are needed to investigate the mechanism

of oxygen level sensing and the driving force leading to a change in the capillary diameter to further understand the mechanism involved in maintaining tissue oxygen homeostasis in the brain.

4. Conclusions

The present study quantified hypoxia-induced restructuring of cerebral microvasculature based on 3D network pathways measured with two-photon microscopy at the same locations within mouse brains over one month. We found that hypoxia-induced vasodilation occurred predominantly in the parenchymal capillaries, indicating that parenchymal capillaries are the major site responding to the chronic hypoxic environment.

Acknowledgments The authors thank Mr. Ryutaro Asaga and Mr. Ryota Sakamoto for their help in the preparation of the experiments. This work was partially supported by Special Coordination Funds for Promoting Science and Technology (K.M.).

References

1. Masamoto K, Tanishita K (2009) Oxygen transport in brain tissue. J Biomech Eng 131: 074002
2. Boero JA, Ascher J, Arregui A et al (1999) Increased brain capillaries in chronic hypoxia. J Appl Physiol 86:1211-1219
3. Xu K, LaManna JC (2006) Chronic hypoxia and the cerebral circulation. J Appl Physiol 100:725-730
4. Wsseling P, Ruiter DJ, Burger PC (1997) Angiogenesis in brain tumors; pathobiological and clinical aspects. J Neurooncol 32:253-265
5. Meyer EP, Ulmann-Schuler A, Staufenbiel M et al (2008) Altered morphology and 3D architecture of brain vasculature in a mouse mode for Alzheimer's disease. Proc Natl Acad Sci U S A 105:3587-3592
6. Denk W, Strickler JH, Webb WW (1990) Two-photon laser scanning fluorescence microscopy. Science 248:73-76
7. So PT, Dong CY, Masters BR et al (2000) Two-photon excitation fluorescence microscopy. Annu Rev Biomed Eng 2:399-429
8. Helmchen F, Denk W (2005) Deep tissue two-photon microscopy. Nat Methods 2:932-940
9. Yamada Y (1995) Light-tissue interaction and optical imaging in biomedicine. Annual Review of Heat Transfer (Begell house, Inc.) 6:1-59
10. Takuwa H, Autio J, Nakayama H et al (2011) Reproducibility and variance of a stimulation-induced hemodynamic response in barrel cortex of awake behaving mice. Brain Res 1369: 103-111

Table 1 Vessel diameter and length measurements of single pathways from a penetrating arteriole (A) to the emerging vein (V) through parenchymal capillaries (C, < 7 μm in diameter) during chronic hypoxia

i) 8% O_2 (n=5)

	Diameter (μm)				Length (μm)			
(total #)	day 0	day 7	day 14	day 21	day 0	day 7	day 14	day 21
A (32)	11±5	14±5	15±5	16±6	77±41	78±39	76±41	77±38
C (61)	4.9±0.9	6.8±1.3	7.5±1.7	8.5±1.9	68±48	69±49	67±46	67±46
V (23)	17±9	21±10	23±12	23±13	91±69	88±66	86±61	81±58

ii) 10% O_2 (n=5)

	Diameter (μm)				Length (μm)			
(total #)	day 0	day 7	day 14	day 21	day 0	day 7	day 14	day 21
A (42)	14±6	17±7	18±7	18±7	126±108	123±108	122±106	123±106
C (69)	5.0±1.0	5.9±1.4	6.4±1.5	6.7±1.8	61±37	62±36	60±36	61±35
V (21)	17±8	19±8	20±9	21±10	136±127	141±122	134±121	133±119

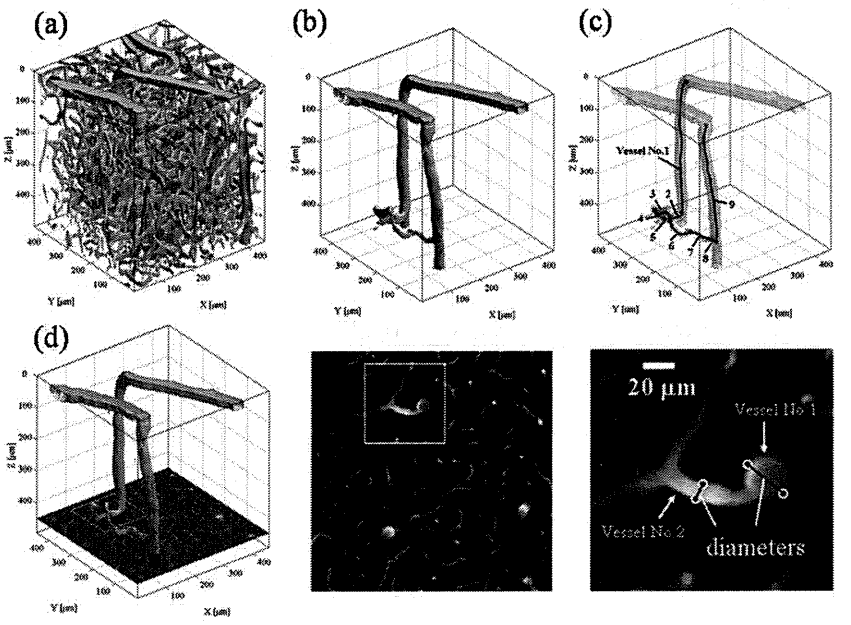

Figure 1. Methods for measuring vessel diameter and length. (a) Reconstructed volume image of parenchymal microvasculature; binarized from 3D image that was reconstructed by rendering obtained 2D x-y images. (b) Selection of a single vessel pathway; the selection criterion was to have the entire connection from the surface arteriole to the surface venule visible within the image. (c) Segmentation and measurement of the length of individual vessel segments. (d) Manual measurement of vessel diameter in the image.